JACS
JOURNAL OF THE AMERICAN CHEMICAL SOCIETY
pubs.acs.org/JACS
Article

Rare-Earth-Free Magnets: Enhancing Magnetic Anisotropy and Spin Exchange Toward High-T_C $Hf_2MIr_5B_2$ (M = Mn, Fe)

Pritam Shankhari, Oliver Janka, Rainer Pöttgen, and Boniface P. T. Fokwa*

Cite This: J. Am. Chem. Soc. 2021, 143, 4205−4212
Read Online
ACCESS | Metrics & More | Article Recommendations | Supporting Information

ABSTRACT: Designing new rare-earth-free (REF) permanent magnetic materials (PMM) to replace the high performing but critically restrained rare-earth-based PMM remains a great challenge to the scientific community. Here, we report on the rational design of new REF PMM, $Hf_2MIr_5B_2$ (M = Fe, Mn) via a theory-experiment combined approach. Density functional theory (DFT) predicted strong interchain M-M spin-exchange coupling and large magnetocrystalline anisotropy energies (E_{MAE}) for the new compounds, suggesting potential intrinsic PMM properties. Subsequent experimental bulk syntheses and magnetic characterizations established the highest ordering temperature (T_C ~ 900 K) for $Hf_2FeIr_5B_2$ and the highest intrinsic coercivity (H_C) value for $Hf_2MnIr_5B_2$ (H_C = 62.1 kA/m) reported to date for $Ti_3Co_5B_2$-type compounds. Importantly, at room temperature both phases show significant coercivities due to intrinsic factors only, hinting at their huge potential to create REF PMM by improving extrinsic factors such as controlling the microstructure and the domain orientation.

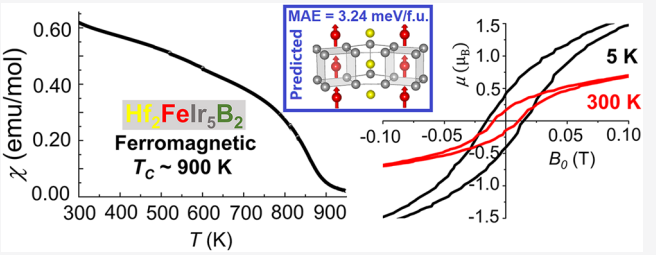

Downloaded via UNIV OF CALIFORNIA RIVERSIDE on December 14, 2021 at 06:52:48 (UTC).
See https://pubs.acs.org/sharingguidelines for options on how to legitimately share published articles.

INTRODUCTION

Rare-earth (RE) elements such as neodymium and samarium are the critical ingredients of today's best-performing permanent magnets like $Nd_2Fe_{14}B$ or $SmCo_5$.[1,2] Another heavy RE, dysprosium, is used as an additive for sustaining the performance of the $Nd_2Fe_{14}B$ magnet at higher temperatures. These RE-based permanent magnetic materials (PMM) exhibit large coercivity (H_c) and remanence (B_r), which result in their large energy products (BH_{max}). On the one hand, magnetic materials with H_c values ≤ 1 kA/m are termed as "soft magnets" and are used in applications where rapid magnetization and demagnetization is required, such as power transformers and magnetic refrigeration.[3,4] On the other hand, magnetic materials showing large coercivity (H_c ≥ 30 kA/m up to several hundred) are termed as "hard magnets" and are used in permanent magnetic applications, such as in energy conversion and power generation.[1,5,6] A recent boom in clean and environmentally friendly technologies, such as electric vehicles and wind turbines, has pushed the demand for high-performing PMM. The Department of Energy (DOE) has marked some RE elements used in the PMM as critical to the U.S.,[7−9] thus there is a growing need to move on from RE-based PMM and develop new rare-earth-free (REF) PMM.

Continuous efforts have been made to discover new REF PMM showing (i) a high ferromagnetic ordering temperature (Curie temperature, T_C), (ii) a large remanence magnetization (B_r), and (iii) a large coercivity (H_c). Although the first two criteria can be met with a REF pure transition metal/intermetallic magnet without any f-electrons, it is the latter requirement that throws a real challenge.[10,11] B_r is an intrinsic property (chemical composition and crystal structure-dependent), while H_c is an intrinsic as well as an extrinsic (microstructure dependent) property of materials. Consequently, the first step in designing a PMM starts with addressing the intrinsic properties, i.e., finding materials with T_C well above room temperature, large B_r, and H_c values. B_r is related to the saturation magnetization (M_S), while H_c depends on the magnetocrystalline anisotropy. The latter refers to the dependence of magnetic energy on the magnetization axis, and it is estimated through the spin−orbit coupling (SOC), using eq 1 for the case of an itinerant ferromagnet:[12]

$$K_1 \approx \pm\frac{1}{4}\zeta\,\Delta L \tag{1}$$

where K_1 is the magnetic anisotropy constant, ζ is the single-electron SOC, and ΔL = anisotropy of the orbital moment, defined as

$$\Delta L = \langle L\rangle M\|Z - \langle L\rangle M\perp Z \tag{2}$$

Since $\zeta \propto Z^2$, the anisotropy generally increases with increasing atomic number (Z).[13] Additionally, the expected values of the orbital moment L for 3d elements are much lower

Received: October 12, 2020
Published: March 9, 2021

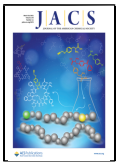

© 2021 American Chemical Society

https://dx.doi.org/10.1021/jacs.0c10778
J. Am. Chem. Soc. 2021, 143, 4205−4212

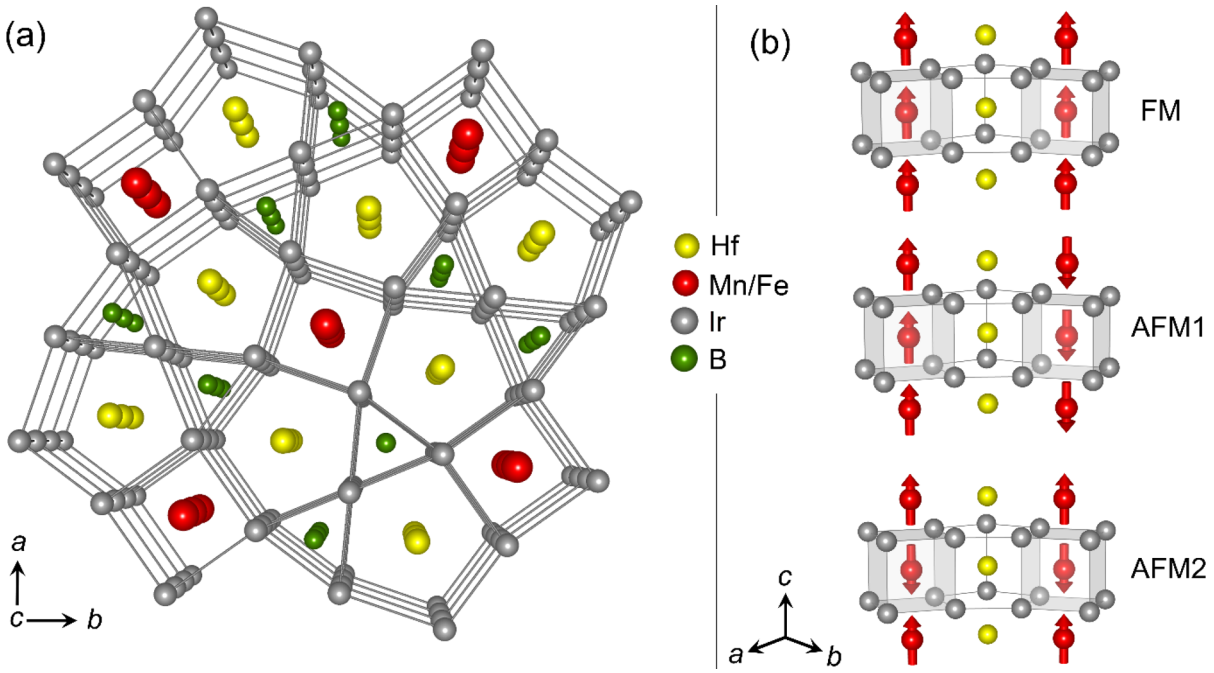

Figure 1. Perspective view of the crystal structure of the quaternaries $Hf_2MIr_5B_2$ (M = Fe, Mn) viewed along [001] (left) and different models of magnetic chains (right).

which makes ΔL small. RE moments, however, are unquenched and show a strong coupling between the 4f charge cloud and the spin, thus materials containing RE have the highest anisotropy values. In contrast, REF materials have intrinsically low SOC values and thus rely on improved extrinsic properties to increase H_c. For example, controlling microstructure and domain orientation has led to appreciable results in Mn-based phases such as binary MnAl and MnBi[14−17] or phases from the systems Zr−Co and Hf−Co,[18−21] and $L1_0$-ordered compounds, such as FeCo, CoPt, FeNi,[22−24] and α''-$Fe_{16}N_2$.[25] These REF PMM have shown large coercivity (H_c values up to several hundred kA/m) and high-ordering temperatures (as high as ∼1000 K). Many of these materials, however, have synthetic, postprocessing, or stability issues. For example, MnBi starts to decompose at 535 K, the metastable nature of MnAl makes it difficult to obtain good texture and high coercivity simultaneously through standard manufacturing methods, and $L1_0$-ordered FeNi and FeCo are difficult to form and their bulk synthesis has not been achieved yet. Thus, designing and preparing new REF compounds showing intrinsically large magnetic anisotropy coupled with issueless bulk synthesis remains a great challenge to the magnetism community.

A few years ago, large H_c values were reported for two members of the transition metal-rich boride series $Sc_2FeRu_{5-x}Ir_xB_2$ [x = 0−5, and number of valence electrons (VE) = 60−65], adopting the tetragonal $Ti_3Co_5B_2$ structure type (space group $P4/mbm$).[26] The 62 and 63 VE members showed intrinsic H_c values up to 52.4 kA/m and were classified as hard magnetic materials but at 5 K (far below room temperature). Following this discovery, *ab initio* density functional theory (DFT) calculations revealed large magneto-crystalline anisotropy energy (E_{MAE}) of −2.85 meV/f.u. in the 62 VE $Sc_2FeRu_3Ir_2B_2$, which originated from its very large SOC energy (E_{SOC} = −2.83 meV/f.u.) with a minor contribution from magnetic dipole−dipole interactions (E_{MDD} = −0.02 meV/f.u.).[27] Although this compound showed a large E_{SOC} value, the spin exchange energy (estimated from the energy difference between ferromagnetic (FM) and antiferromagnetic (AFM) spin orientations) showed the presence of competing FM and AFM interactions with dominating AFM interactions, which resulted in very small magnetization (0.45 μ_B/f.u.) for this compound. While these phases show great potential in intrinsic properties, they can only become attractive for future REF magnetic applications if the FM interactions and ordering temperatures (ideally above room temperature) are drastically increased by simultaneously maintaining or increasing E_{MAE}. Recent studies of the magnetic properties of the $Ti_3Co_5B_2$-type intermetallic compounds have shown that FM interactions dominate AFM ones at higher VE numbers. Furthermore, according to the above discussion on the SOC requirement of a large atomic number, introducing more 5d elements should help in increasing the E_{MAE}. Consequently, we have replaced Sc (3d element) and Ru (4d element) in $Sc_2FeRu_3Ir_2B_2$ by the 5d elements Hf and Ir, respectively, to generate the 67 VE phase $Hf_2FeIr_5B_2$. Further substitution of Mn for Fe then generates the 66 VE phase $Hf_2MnIr_5B_2$. Herein, we report on the design of the first REF borides, $Hf_2MnIr_5B_2$ and $Hf_2FeIr_5B_2$, showing high Tc values (590 and 900 K, respectively) as well as high intrinsic H_c values in the semihard range above room temperature (13.0 and 8.9 kA/m at 300 K, respectively). Ab initio DFT calculations followed by experimental studies of these 2 new phases with respect to their compositions, structures, and magnetic properties are presented below.

COMPUTATIONAL RESULTS AND DISCUSSION

The procedure to design the new compounds was clear: maximize the number of 5d elements in an anisotropic crystal structure. The recently published $Sc_2FeRu_3Ir_2B_2$ crystallizes in the tetragonal $Ti_3Co_5B_2$ structure type with $a/c \sim 2.8$.[26] Thus, we envisioned the new quaternaries $Hf_2MIr_5B_2$ (M = Fe, Mn)

https://dx.doi.org/10.1021/jacs.0c10778
J. Am. Chem. Soc. 2021, 143, 4205−4212

by replacing the lighter Sc (3d element) and Ru (4d element) in $Sc_2FeRu_3Ir_2B_2$ by the heavier 5d elements Hf and Ir, respectively. The crystal structures of the newly designed quaternaries are built by face-connected trigonal, tetragonal, and pentagonal prisms of Ir atoms (Figure 1). The large Hf atoms reside inside the pentagonal prisms, whereas the small B atoms are located within the trigonal prisms and the *M* atoms are found in the tetragonal prisms. DFT calculations were used to investigate the stability, electronic structure, and spin orientations of the envisioned compounds. The lattice parameters were relaxed using the projector augmented wave method of Blöchl[28−30] coded in the Vienna *ab initio* simulation package (VASP).[31] All VASP calculations employed the generalized gradient approximation (GGA) with the Perdew-Burke-Enzerhoff (PBE) functional.[32] The cutoff energy for the plane wave calculations was set to 500 eV. The Brillouin zone integrations were carried out using a 5 × 5 × 15 *k*-point mesh for the nonmagnetic, FM, and AFM1 models for both compounds, whereas a 5 × 5 × 7 *k*-point mesh was used for the $a \times a \times 2c$ supercell (AFM2 model).

Density of States. We recently reported on the electronic structure of the ternary $Hf_3Ir_5B_2$ where the nonspin-polarized (nsp) density of states (DOS) plot shows a large pseudogap around the Fermi level (E_F).[33] The large pseudogap found around E_F is a typical feature of the $Ti_3Co_5B_2$ structure type which indicates electronic stability.[34,35] Upon replacing one Hf atom per sum formula with the magnetic *M* resulting in $Hf_2MIr_5B_2$, the corresponding DOS increases sharply at E_F and the pseudogap feature is lost. Instead, as shown in Figure 2a,b, due to the *M* atoms a large peak appeared at E_F (contributions due to *M* atoms are shown in dotted lines) indicating

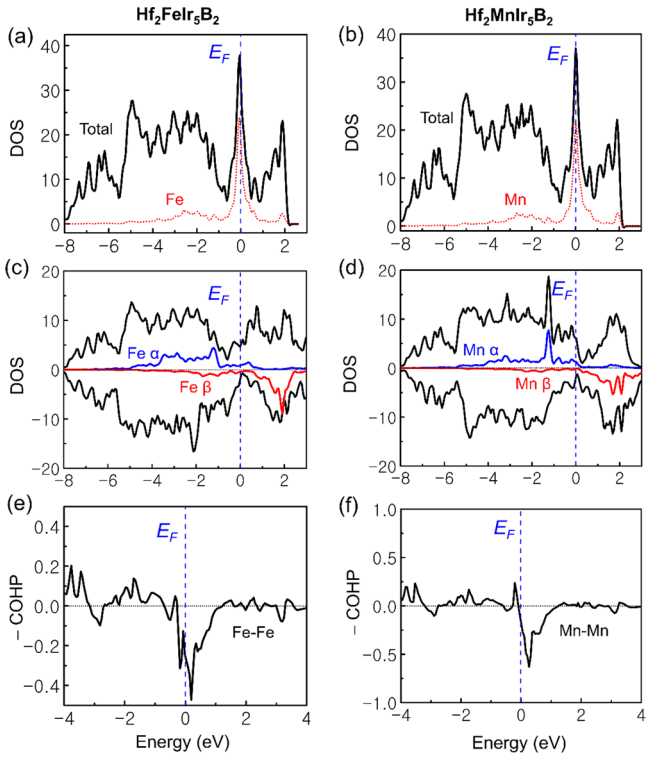

Figure 2. Nonspin-polarized DOS plots (a,b), spin-polarized DOS plots (c,d) and nonspin-polarized −COHP plots (e,f) for *M*−*M* interaction along [001] in $Hf_2FeIr_5B_2$ (M = Fe) and $Hf_2MnIr_5B_2$ (M = Mn).

electronic instability. For the predicted quaternaries to be stable, this electronic instability must be compensated, in this case through magnetic interactions. Indeed, the peaks at E_F disappeared upon spin-polarization giving rise to the plots shown in Figure 2c,d. Partial DOS plots showed that Fe and Mn are mainly responsible for the spin-polarization as their DOSs produced the largest spin split (α and β) of all elements involved, suggesting that magnetism should be responsible for this electronic stabilization, so we moved on to study different magnetic models and compared them to the nonmagnetic (NM) case.

Spin-Exchange Energy and COHP. The placement of the magnetic *M* atoms at the 2*a Wyckoff* site generates *M* chains along the crystallographic [001] direction (Figure 1). Three different magnetic models, namely, FM, AFM1, and AFM2, as previously done for $Hf_2MnRu_5B_2$[36] were considered (Figure 1, right) to estimate the spin-exchange energies. The resulting VASP total energies of these three magnetic models and the magnetic moments of the FM model are given in Table S1 and Table S2 of the Supporting Information. All magnetic models for both compounds were at least 1.1 eV/f.u. more stable than the corresponding NM model, indicating that magnetic ordering is highly likely. The predicted spin interactions in the two compounds are quite different: while FM is predicted to be the ground state for $Hf_2FeIr_5B_2$ by 40 meV/f.u. over AFM1, $Hf_2MnIr_5B_2$ is predicted to order with an AFM1 ground state by 60 meV/f.u. over FM. Interestingly, both FM and AFM1 models consist of FM chains of *M* (Fe, Mn) that are separated from each other by a large distance of ∼6.5 Å, indicating that the interchain interactions, which differentiate both models are dominated by conduction electrons. Consequently, the similarity in stabilization energies confirms that these interchain interactions are rather weak, thus they can easily be affected by external stimuli such as magnetic field or pressure. This finding corroborates our recent report on the Ru-based series $A_2MRu_5B_2$ (*A* = Zr, Hf and M = Fe, Mn),[37] the magnetic orderings of which were found to be highly magnetic-field-dependent. While the predicted FM ground state is in perfect agreement for $Hf_2FeIr_5B_2$, if compared with previously reported $Ti_3Co_5B_2$-type compounds (Table S2), AFM1 is somewhat unexpected for $Hf_2MnIr_5B_2$. In fact, AFM1 is mostly preferred in Fe-based Ru-rich compounds with 63 VE or fewer, while FM is more stable for phases that are richer in group-9-elements (Co, Rh, and Ir) and have 63 VE or more. Examples of calculated AFM1 compounds include: $Sc_2FeRu_{5-n}Ir_nB_2$ (n = 0−2; 60−62 VE),[27] $Zr_2FeRu_5B_2$ (62 VE),[37] $Hf_2FeRu_5B_2$ (62 VE),[37] $Ti_2FeRu_4RhB_2$ (63 VE),[27] and $Sc_2FeRu_3Ir_2B_2$ (62 VE),[27] while the calculated FM compounds are $Sc_2FeRu_{5-n}Ir_nB_2$ (n = 3−5; 63−65 VE),[27] $Hf_2FeIr_5B_2$ (67 VE, present work), $Ti_2FeRh_5B_2$ (67 VE),[27] $Ti_2FeCo_5B_2$ (67 VE),[27] and $Hf_2FeCo_5B_2$ (67 VE).[27]

In contrast to the Fe-based compounds, the five Mn-based compounds calculated so far do not show a VE-dependent trend: while $Hf_2MnRu_5B_2$ (61 VE) and $Hf_2MnCo_5B_2$ (66 VE) have FM ground state, the remaining three compounds $Zr_2MnRu_5B_2$ (61 VE), $Ti_2MnCo_5B_2$ (66 VE), and $Hf_2MnIr_5B_2$ (66 VE, present work) prefer AFM1 ground state, making all Mn-based phases highly unpredictable. Therefore, it is impossible to draw a conclusion on the trend of the Mn-based compounds, and thus it is better to treat the Fe- and Mn-based compounds separately.

In addition to the spin interaction analysis through VASP calculations, crystal orbital Hamilton population (COHP)[38]

https://dx.doi.org/10.1021/jacs.0c10778
J. Am. Chem. Soc. 2021, 143, 4205−4212

Table 1. E_{SOC} ($E_{SOC} \parallel c - E_{SOC} \perp c$), Exchange Energy E_{ex} ($E_{AFM1} - E_{FM}$), Coercivity, and Magnetic Moments of $Hf_2MIr_5B_2$ (M = Fe, Mn) and Some Other Reported $Ti_3Co_5B_2$-Type Compounds

compound	E_{ex} (meV/f.u.)	E_{SOC} (meV/f.u.)	H_C (kAm/m)	μ_a (μ_B), at B_0(T)	reference
$Hf_2FeIr_5B_2$	+40.19	+3.27	12.1	3.2, 8.0	this work
$Hf_2MnIr_5B_2$	−60.01	−1.55	62.0	0.8, 8.0	this work
$Sc_2FeRu_3Ir_2B_2$	−36.77	−2.83	51.6	0.09, 5.0	27
$Ti_2FeRu_4RhB_2$	−30.55	−0.23	23.9	0.6, 4.5	27
$Ti_2FeRh_5B_2$	+3.74	−0.18	0.9	2.3, 4.5	27
$Ti_2FeCo_5B_2$	+53.09	+0.14	–	–	27
Hf_2FeCo_5B2	+58.88	+0.20	–	–	27
$Hf_2MnRu_5B_2$	+1.92	+0.42	–	–	36
$Ti_2MnCo_5B_2$	−9.82	+0.12	–	–	27
$Hf_2MnCo_5B_2$	+5.46	+0.99	–	–	27

analysis was performed, using the TB-LMTO method (Stuttgart version of the tight-binding linear muffin-tin orbital with the atomic spheres approximation)[39] in order to verify the VASP-predicted FM intrachain interactions within the *M* chains. According to the COHP methodology, FM interactions would place E_F in an antibonding region while for AFM it would be placed in a nonbonding region.[40] The −COHP plots for Fe−Fe and Mn−Mn interactions in their respective compounds are given in Figure 2e,f. Indeed, E_F is placed in an antibonding region for both −COHP curves, thus confirming the presence of ferromagnetic intrachain *M*−*M* spin interactions in both compounds.

Spin−Orbit Coupling. Given the fact that both compounds have strong FM intrachain interactions and rather weak interchain magnetic interactions, they are ideal candidates for intrinsic magnetic anisotropy. We have therefore examined the SOC contribution toward the total E_{MAE} by applying GGA+SOC calculations as described by Zhang et al.[27] for calculations within the $Ti_3Co_5B_2$-type structure. There are two contributions toward the total E_{MAE}: (i) single-element magnetic anisotropy energy (E_{SOC}) that arises from SOC and (ii) long-range magnetic dipole−dipole (MDD) interaction energy (E_{MDD}). VASP total energies of spin parallel ($E_{SOC} \parallel c$) and spin perpendicular ($E_{SOC} \perp c$) to the crystallographic *c*-axis for each compound were calculated. The net E_{SOC} was then calculated using eq 3

$$E_{SOC} = E_{SOC}\|c - E_{SOC}\perp c \quad (3)$$

$$E_{MAE} = E_{SOC} + E_{MDD} \quad (4)$$

$$E_{MAE} \approx E_{SOC} \quad (5)$$

The results of the E_{SOC} calculations are given in Table 1 along with the E_{SOC} of some other reported compounds of the same structure type. Since the contribution of E_{MDD} toward the total E_{MAE} is small, typically in the order of 10^{-2} meV/f.u., we have ignored it in eq 5 and approximated $E_{MAE} \approx E_{SOC}$.

Besides, the interchain *M*−*M* distances in $Ti_3Co_5B_2$-type phases are large, thus the nature (FM vs AFM1) and strength of interchain spin-exchange (through conduction electrons) will also affect the coercive field H_C, especially a strong AFM spin-exchange would require an additional magnetic field to flip the opposite spins to the field direction. The spin-exchange strength can be rationalized by comparing the electronic energies of the FM and AFM1 states ($E_{ex} = E_{AFM1} - E_{FM}$).

The calculated E_{SOC} (+3.27 meV/f.u.) for FM $Hf_2FeIr_5B_2$ is larger than all values reported so far for $Ti_3Co_5B_2$-type phases (Table 1), indicating a large magnetic anisotropy in which spin ⊥ *c* (easy plane) is favored, thus making $Hf_2FeIr_5B_2$ a good REF magnet candidate. Interestingly, $Hf_2MnIr_5B_2$, which prefers an AFM1 ordering also shows the third highest E_{SOC} value (−1.55 meV/f.u.) of all $Ti_3Co_5B_2$-type phases and has an easy *c* axis. Moreover, it has an exchange energy larger (E_{ex} = −60.01 meV/f.u.) than that of hard-magnetic $Sc_2FeRu_3Ir_2B_2$ (E_{ex} = −36.77 meV/f.u.), thus $Hf_2MnIr_5B_2$ is predicted to also be a REF magnet candidate. Given that most REF hard magnetic materials have far smaller E_{SOC} values such as −0.15 meV/f.u. for MnBi, there is a high chance that the predicted intrinsic hard magnetic properties for these new phases can be realized (see the Experimental Results below).

EXPERIMENTAL RESULTS AND DISCUSSION

Phase Analysis and Structure Determination. The two new compounds were synthesized by arc-melting elemental mixtures in an argon atmosphere and characterized by powder X-ray diffraction (PXRD) and energy-dispersive X-ray spectroscopy (EDS), as detailed in the Supporting Information. The *Rietveld* refinement results of both compounds obtained using the *FullProf* program package[41,42] are given in Tables S4 and S5 and Figures S1 and S2). The refinements confirmed the presence of the $Ti_3Co_5B_2$-type structure (space group *P*4/*mbm*) as the main phase and $HfIr_3B_{0.5}$ as a side phase. The refined lattice parameters, *a* = 9.0969(7) and *c* = 3.2039(3) Å for $Hf_2FeIr_5B_2$, are smaller than those of $Hf_2MnIr_5B_2$ [*a* = 9.1845(6) and *c* = 3.2146(3) Å], in agreement with the smaller Fe atomic radius if compared to that of Mn. Furthermore, the refined lattice parameters of both phases are smaller than those [*a* = 9.264(2), *c* = 3.3070(5) Å] of reported $Hf_3Ir_5B_2$[33] because the larger Hf atoms are replaced by the smaller Mn/Fe atoms. Next, we carefully quantified the site occupancies at different *Wyckoff* positions by refining mixed occupancies. Many reported isotypic compounds are known to show mixed occupancies at the 2*a* site, for example in $Hf_2Mn_{1-x}Ru_{5+x}B_2$,[36] and $Zr_2Fe_{1-x}Ru_{5+x}B_2$,[43] the 2*a* site was occupied by a Ru/*M* (*M* = Mn, Fe) mixture, whereas in $Hf_3Ir_5B_2$, this site is occupied by Hf only. Consequently, we have evaluated possibilities of both Hf/*M* and Ir/*M* mixed occupancy refinements at the 2*a* site. The refinements were carried out following the same procedure for the 2 phases, thus we will detail only one of them. We started with 100% Mn at site 2*a* (corresponding to $Hf_2MnIr_5B_2$) and refined the occupancy freely which led to an excess electron density, thus hinting at the presence of an element with higher electron density (either Hf or Ir). Next, we refined Hf/Mn and Ir/Mn mixed occupancies at the 2*a* site separately. Interestingly, both Hf and Ir could be incorporated at site 2*a* leading to the compositions $Hf_{2.22}Mn_{0.78}Ir_5B_2$ (composition 1) and $Hf_2Mn_{0.82}Ir_{5.18}B_2$ (composition 2), respectively. To check which of these two compositions was correct, we fixed the Mn's site occupancy factor (SOF) and refined those of Hf and Ir at 2*a* simultaneously. Interestingly, this refinement step led to a positive SOF for Ir (0.038) and a negative SOF for Hf (−0.010). Consequently, Ir is clearly preferred at the 2*a* site (along with Mn) compared to Hf. Further mixed occupancy refinements using Ir/Hr or Ir/Mn at the Ir sites 2*c* and 8*j* were unsuccessful, and free refinements

https://dx.doi.org/10.1021/jacs.0c10778
J. Am. Chem. Soc. 2021, 143, 4205−4212

of the SOF of these sites did not lead to a significant change in composition. The Fe-based compound indicated the same refinement behavior as the Mn-based one. The final refinement results led to the compositions $Hf_2Fe_{0.64(2)}Ir_{5.36(2)}B_2$ and $Hf_2Mn_{0.82(2)}Ir_{5.18(2)}B_2$, with good R-values. The metal composition was semiquantitively analyzed by EDS (Figures S3 and S4), the results which unambiguously confirm excess Ir (not excess Hf) in the compounds in accordance with refinement results. We note that the displacement parameters could not be refined simultaneously and thus they were fixed during these refinements. Additionally, both compounds were produced with the cubic phase $HfIr_3B_{0.5}$ (Table S4). Although, this compound is not expected to be magnetically ordered, the presence of Fe/Mn could change its magnetic properties, thus we have checked for the possible presence of Fe/Mn in this perovskite phase. Even though Mn/Fe could be refined on the Ir site using mixed occupancy refinement, no change of the *R*-values was found and the refined SOF of Mn/Fe was zero within standard deviation. Also, a few small unmatched peaks are seen in the refinement around 28, 32, and 47 deg. which are from oxides of Hf always present in the PXRD when synthesizing Hf-based compounds, including the nonmagnetic $Hf_3Ru_5B_2$ or $Hf_3Ir_5B_2$.[33] Therefore, there should not be any other magnetic impurities of concern which would produce such strong magnetic interactions observed from the title compounds (see later).

Magnetization Results and Discussion. The magnetic susceptibility (χ) was measured in zero-field-cooled mode at 1.0 T as a function of temperature (T) on polycrystalline samples of $Hf_2FeIr_5B_2$ (temperature range 3−950 K) and $Hf_2MnIr_5B_2$ (temperature range 3−650 K). As expected for these samples synthesized by arc-melting above 2770 K, the samples remain crystalline after the high temperature magnetic measurements as exemplified by the PXRD of the Mn-based phase (Figure S5). The high temperature χ-T plots (Figure 3a,c) for $Hf_2FeIr_5B_2$ and $Hf_2MnIr_5B_2$ have a typical

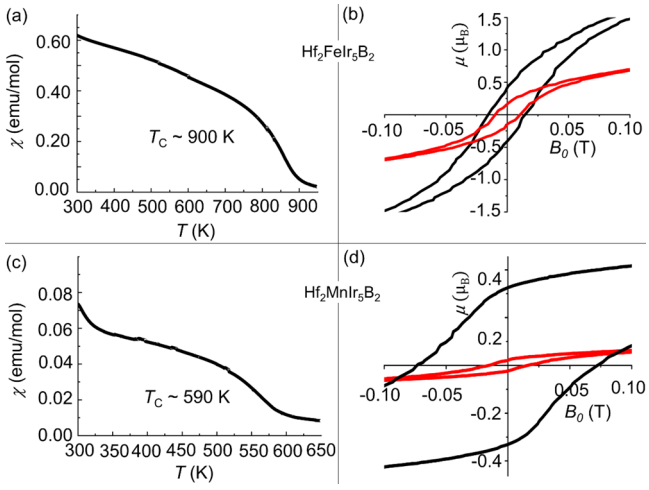

Figure 3. Magnetic susceptibility as a function of temperature measured at 1.0 T for $Hf_2FeIr_5B_2$ (a) and $Hf_2MnIr_5B_2$ (c). Hysteresis loop measured at 5 K (black) and 300 K (red) for $Hf_2FeIr_5B_2$ (b) and $Hf_2MnIr_5B_2$ (d).

behavior of a ferromagnet, showing a sharp transition at the Curie temperature (T_C). T_C values of ~900 and ~590 K were estimated for $Hf_2FeIr_5B_2$ and $Hf_2MnIr_5B_2$, respectively, using the line projection method.[44]

While DFT predicted FM ordering for the Fe-based phase, an AFM ordering for the Mn-based phase was predicted instead. However, the energy difference between FM and AFM1 was relatively small (40 and 60 meV) indicating that a high magnetic field can alter the AFM Mn−Mn interchain interactions. Indeed, at lower temperatures, a maximum was observed at 30 K, indicating a Néel temperature (T_N) and confirming the AFM order predicted at 0 K by DFT calculations. Furthermore, increasing the magnetic field to 8.0 T destroys the maximum (Figure S6). Recently, we discovered $Hf_2MnRu_5B_2$, which also orders antiferromagnetically with T_N = 20 K. However, in $Hf_2MnRu_5B_2$ the AFM interactions are very weak and a smaller field as low as 1.0 T was enough to destroy this AFM ordering in favor of FM ordering. These results confirm the VASP calculations which have predicted an AFM ground state for $Hf_2MnIr_5B_2$ (this work) but a competition between FM and AFM1 ground states for $Hf_2MnRu_5B_2$.[36] However, just like $Hf_2MnRu_5B_2$ and most AFM-based phases in this compound family, the interchain AFM interactions may be affected by the magnetic field or the temperature, leading to metamagnetic behavior. Nevertheless, the low-temperature behavior (below RT) of these compounds should be further investigated in detail in the future, as both χ-T plots show an unusual increase in susceptibility. For the present work, the hysteresis behavior is more important as both compounds have been predicted to be potential hard magnets. Field-dependent magnetization (μ-H) was measured at different temperatures and up to 8.0 T (Figure S7). The μ-H plots are given in Figure 3b,d. Refined compositions (Table S4) were used to calculate all the magnetic moments presented here. The magnetization of $Hf_2FeIr_5B_2$ measured at 3 K rose rapidly as the applied field was increased and reached near-saturation at about 3.0 T. Further increasing the field up to 8.0 T only resulted in a slight increase in the magnetic moment where it reached a maximum value of 3.2 μ_B/f.u. This moment is somewhat close to the calculated total moment (3.62 μ_B/f.u.) of the compound in the FM model (Table S2), considering that saturation is not yet reached. The magnetization of $HfMnIr_5B_2$ at 3 K rapidly increased but did not saturate even at 8.0 T, reaching a magnetic moment of only 0.8 μ_B/f.u. This small moment value, if compared to that calculated for an FM state (3.83 μ_B/f.u., Table S2) clearly shows that AFM interactions are present, thus indicating a metamagnetic behavior for $HfMnIr_5B_2$. Additionally, the mixing of M/Ir at site 2*a* has likely lowered the total magnetic moment of both compounds.

The T_C value (590 K) of $Hf_2MnRu_5B_2$ is close to the values (546 and 579 K) reported in two recent studies for orthorhombic β-MnB.[45,46] Hence, we specifically investigated the presence of β-MnB in our arc-melted 2Hf-Mn-5Ir-2B product since Mn and B are part of the starting materials. The simulated peaks for orthorhombic β-MnB could not be identified in the measured PXRD data of the product. Nevertheless, we also performed a *Rietveld* refinement of the PXRD data by adding β-MnB as a side phase and fixing all other phases and parameters. However, the refinement did not converge, thus further hinting at the absence of β-MnB. Moreover, we recently reported on compounds that were arc-melted from similar stoichiometries 2Hf-Mn-5Ru-2B and 2Zr-Mn-5Ru-2B. Even though Mn and B were present, no ferromagnetic behavior was observed at high temperature. Lastly, β-MnB shows nearly zero coercivity at 5 K,[45,46] while hysteresis loops measured for $Hf_2MnRu_5B_2$ show large coercivity and hysteresis (see next section). These studies unambiguously demonstrate the absence of β-MnB, therefore the magnetic data represented here are solely due to the newly synthesized $Hf_2MnIr_5B_2$.

Hysteresis Loop and Coercivity. Figure S8 shows the hysteresis loops for the new compounds measured at 5 and 300 K, up to a magnetic field of 2 T. Figure 3b,d shows the enlarged sections of the hysteresis loops, indicating coercivity (H_c) values at 5 K of 12.1 and 62.0 kA/m for $Hf_2FeIr_5B_2$ and $Hf_2MnIr_5B_2$, respectively. These values classify the Fe-based phase as a semihard magnetic material and the Mn-based one as a hard-magnetic material at 5 K. These findings confirm the DFT predictions only for $Hf_2MnIr_5B_2$, suggesting that the presence of AFM interchain interactions (stronger in $Hf_2MnIr_5B_2$) is a key factor in predicting the intrinsic magnetic anisotropy of these materials. Nevertheless, the high-ordering temperature (900 K) and large saturation magnetization of $Hf_2FeIr_5B_2$ make it a good REF magnetic material candidate. The H_C value recorded for $Hf_2MnIr_5B_2$ is ~10 kA/m larger than the highest value so far reported for this structure type (52.4 kA/m $Sc_2FeRu_2Ir_3B_2$), thus making this new phase the best low-temperature REF PMM so far reported in structure type. Interestingly, slightly above room temperature (300 K), H_c for the 2 new phases is still significant with values of 8.9 and 13.0 kA/m for $Hf_2FeIr_5B_2$ and $Hf_2MnIr_5B_2$, respectively. This is a

https://dx.doi.org/10.1021/jacs.0c10778
J. Am. Chem. Soc. 2021, 143, 4205−4212

significant finding for this structure type because all H_c values have been obtained at far lower temperatures (<10 K) and most of these materials (such as $Sc_2FeRu_2Ir_3B_2$) become paramagnetic at room temperature.[26] Consequently, $Hf_2MIr_5B_2$ (M = Fe, Mn) are the first $Ti_3Co_5B_2$-type compounds to show both high H_c values and above room temperature ordering, thus placing them in a unique position for the realization of REF magnets.

Balance between Large Coercivity and High Magnetic Moment. For $Hf_2MnIr_5B_2$, the Mn−Mn interchain coupling is strongly antiferromagnetic as AFM1 is 60.01 meV/f.u. energetically more favorable than FM. This strong interchain spin-exchange interaction makes it difficult to flip the spins of Mn chains under an applied magnetic field, giving rise to a large coercivity value. A similar situation was observed for some other compounds showing coercivity values in the semihard to hard region, as presented in Table 1. Such compounds include $Sc_2FeRu_3Ir_2B_2$, $Ti_2FeRu_4RhB_2$, and $Hf_2MnIr_5B_2$ where strong interchain spin-exchange interactions are present. Although these compounds show high coercivities, the presence of significant antiferromagnetic interactions in some of these compounds (AFM1 ground state) results in smaller total magnetic moments (see Table 1). If the interchain spin-exchange interaction is weak then it is easy to flip the spins of *M* chains under an applied magnetic field, for example $Ti_2FeRh_5B_2$, which has weak interchain interaction as FM is only +3.74 meV/f.u. more stable than AFM1. In this compound, FM interactions dominate, which results in its large total magnetic moment of 2.3 μ_B. An interesting entry is the new phase $Hf_2FeIr_5B_2$, which has strong FM interchain spin-exchange interaction as FM is more stable than AFM1 by 40.19 meV/f.u. Due to this strong interaction between the chains, the chains are in a locked position, thus nearby chains prevent flipping of individual spins of a chain leading to its large H_c value. The absence of AFM interactions or the presence of strong FM interactions results in the large total magnetic moment of 3.2 μ_B for this compound. In fact, the FM coupling between the spins are so strong in this compound that remarkably high thermal energy is required to randomize the spins ($T_c \sim 900$ K).

Perspectives: Extrinsic Properties. As far as the magnetic properties are concerned, the newly synthesized compounds fall in the intermediate range of the H_c spectrum, but they show remarkably high ordering temperatures as well as chemical and thermal stabilities. Both compounds are thermally stable as they were synthesized at ca. 3270 K and can withstand harsh chemical environments like concentrated HCl at room temperature for several days. It is worth mentioning that the magnetic measurements of the new compounds were performed on as-synthesized powder samples (micrometer-sized) obtained from crushing a bulk ingot without any further processing, hence the magnetic properties observed are purely intrinsic. Most of the REF magnetic materials discussed in the introduction, however, show their superior magnetic properties only in a highly processed state like ball-milling (particle size reduction), thin film production, sintering, melt-spinning, or densification.[10,18−21] These additional processing techniques can hugely improve the extrinsic magnetic hardness. For example, the high-temperature hard ferromagnetic Hf−Co and Zr−Co alloys were initially prepared using the same arc-melting technique that we have used. Following the arc melting, the alloys were then remelted to a molten state and then melt-spun to form nanocrystalline ribbons which then drastically improve their magnetic properties.[21] The melt-spun ribbon of another intermetallic "$Hf_2Co_{11}B$" with a spin rate of 24 m/s showed soft ferromagnetism with $H_c \leq 10$ Oe. The same compound, melt-spun at a spin rate of 16 m/s showed coercivity values as high as 4500 Oe (358.1 kA/m).[19] Thus, the two newly synthesized materials have an enormous potential if one of the above-mentioned processing methods can be successfully applied to improve their microstructures. Such studies are planned for the near future.

CONCLUSIONS

Ab initio DFT calculations were used to design the new REF magnetic compounds $Hf_2MIr_5B_2$ (*M* = Fe, Mn). Their predicted structural stability, magnetic interactions, and magnetocrystalline anisotropy energy (E_{MAE}) were then evaluated experimentally. The predicted lattice parameters and crystal structures were confirmed experimentally by Rietveld refinements of the powder X-ray diffraction data. FM intrachain *M*−*M* interactions were predicted for both compounds, while AFM and FM interchain *M*−*M* interactions were predicted for $Hf_2MnIr_5B_2$ and $Hf_2FeIr_5B_2$, respectively, indicating metamagnetic behavior for the former and ferromagnetic behavior for the latter. Magnetization measurements confirmed the predicted metamagnetic and ferromagnetic behaviors, leading to two ordering temperatures for $Hf_2MnIr_5B_2$ (T_C = 590 and T_N = 30 K) and only one ordering temperature for $Hf_2FeIr_5B_2$ (T_C = 900 K). Magnetocrystalline anisotropy studies predicted large spin−orbit-coupling energy for both compounds with easy axis anisotropy for M = Fe phase and easy plane for M = Mn. The recorded large hysteresis with coercivity (H_c) values at 5 K of 12.1 and 62.0 kA/m for $Hf_2FeIr_5B_2$ and $Hf_2MnIr_5B_2$, respectively, confirm the predicted large magnetocrystalline anisotropy behavior of both phases. In addition, $Hf_2FeIr_5B_2$ has a high saturation magnetic moment of 3.2 μ_B, a further confirmation of its FM ordering. Importantly, both phases still show significant hysteresis slightly above room temperature, a prerequisite for future application as permanent magnetic materials.

ASSOCIATED CONTENT

Supporting Information

The Supporting Information is available free of charge at https://pubs.acs.org/doi/10.1021/jacs.0c10778.

Experimental procedure for synthesis and characterization of the new compounds (Experimental Procedure), relative energies of different magnetic models as obtained from VASP calculations (Tables S1−S3), Rietveld refinements of powder XRD data (Tables S4 and S5, Figures S1, S2 and S5), SEM and EDS analysis (Figures S3 and S4), low temperature magnetic measurements (Figure S6), field dependent magnetic measurements (Figure S7), and hysteresis loops (Figure S8) (PDF)

AUTHOR INFORMATION

Corresponding Author

Boniface P. T. Fokwa − *Department of Chemistry and Department of Chemical and Environmental Engineering, University of California, Riverside, California 92521, United States;* orcid.org/0000-0001-9802-7815; Email: bfokwa@ucr.edu

Authors

Pritam Shankhari − *Department of Chemistry, University of California, Riverside, California 92521, United States;* orcid.org/0000-0002-8727-0251

Oliver Janka − *Anorganische Festkörperchemie, Universität des Saarlandes, D-66123 Saarbrücken, Germany; Institut für Anorganische und Analytische Chemie, Westfälische Wilhelms-Universität Münster, D-48149 Münster, Germany;* orcid.org/0000-0002-9480-3888

Rainer Pöttgen − *Institut für Anorganische und Analytische Chemie, Westfälische Wilhelms-Universität Münster, D-48149 Münster, Germany*

Complete contact information is available at: https://pubs.acs.org/10.1021/jacs.0c10778

https://dx.doi.org/10.1021/jacs.0c10778
J. Am. Chem. Soc. 2021, 143, 4205−4212

Notes

The authors declare no competing financial interest.

■ ACKNOWLEDGMENTS

This work was supported by the National Science Foundation Career award to BPTF (no. DMR-1654780). The authors also gratefully acknowledge the San Diego Supercomputer Center (SDSC) for providing computing resources. O.L. thanks Saarland University and the German Research Foundation (project number INST 256/349-1) for financial support though the X-ray Diffraction Service Center.

■ REFERENCES

(1) Gutfleisch, O.; Willard, M. A.; Brück, E.; Chen, C. H.; Sankar, S. G.; Liu, J. P. Magnetic materials and devices for the 21st century: stronger, lighter, and more energy efficient. *Adv. Mater.* **2011**, *23* (7), 821−842.

(2) Coey, J. M. Magnetism and Magnetic Materials. Cambridge University Press: Cambridge, U.K., 2010; p 624.

(3) Fish, G. E. Soft magnetic materials. *Proc. IEEE* **1990**, *78* (6), 947−972.

(4) Tan, X.; Chai, P.; Thompson, C. M.; Shatruk, M. Magnetocaloric effect in $AlFe_2B_2$: toward magnetic refrigerants from earth-abundant elements. *J. Am. Chem. Soc.* **2013**, *135* (25), 9553−9557.

(5) Lewis, L. H.; Jimenez-Villacorta, F. Perspectives on Permanent Magnetic Materials for Energy Conversion and Power Generation. *Metall. Mater. Trans. A* **2013**, *44*, 2−20.

(6) Habib, K.; Wenzel, H. Exploring rare earths supply constraints for the emerging clean energy technologies and the role of recycling. *J. Cleaner Prod.* **2014**, *84*, 348−359.

(7) Hoenderdaal, S.; Tercero Espinoza, L.; Marscheider-Weidemann, F.; Graus, W. Can a dysprosium shortage threaten green energy technologies? *Energy* **2013**, *49*, 344−355.

(8) Mancheri, N. A. World trade in rare earths, Chinese export restrictions, and implications. *Resour. Policy* **2015**, *46*, 262−271.

(9) US Department of Energy: *Critical Materials Strategy*, 2011.

(10) Cui, J.; Kramer, M.; Zhou, L.; Liu, F.; Gabay, A.; Hadjipanayis, G.; Balasubramanian, B.; Sellmyer, D. Current progress and future challenges in rare-earth-free permanent magnets. *Acta Mater.* **2018**, *158*, 118−137.

(11) Skomski, R.; Manchanda, P.; Kumar, P.; Balamurugan, B.; Kashyap, A.; Sellmyer, D. J. Predicting the future of permanent-magnet materials. *IEEE Trans. Magn.* **2013**, *49* (7), 3215−3220.

(12) Kuz'Min, M. D.; Skokov, K. P.; Jian, H.; Radulov, I.; Gutfleisch, O. Towards high-performance permanent magnets without rare earths. *J. Phys.: Condens. Matter* **2014**, *26* (6), 064205.

(13) Skokov, K. P.; Gutfleisch, O. Heavy rare earth free, free rare earth and rare earth free magnets-vision and reality. *Scr. Mater.* **2018**, *154*, 289−294.

(14) Cui, J.; Choi, J. P.; Li, G.; Polikarpov, E.; Darsell, J.; Overman, N.; Kramer, M. J. Thermal stability of MnBi magnetic materials. *J. Phys.: Condens. Matter* **2014**, *26*, 064212.

(15) Xie, W.; Polikarpov, E.; Choi, J. P.; Bowden, M. E.; Sun, K.; Cui, J. Effect of ball milling and heat treatment process on MnBi powders magnetic properties. *J. Alloys Compd.* **2016**, *680*, 1−5.

(16) Patel, K.; Zhang, J.; Ren, S. Rare-earth-free high energy product manganese-based magnetic materials. *Nanoscale* **2018**, *10* (25), 11701−11718.

(17) Ly, V.; Wu, X.; Smillie, L.; Shoji, T.; Kato, A.; Manabe, A.; Suzuki, K. Low-temperature phase MnBi compound: A potential candidate for rare-earth free permanent magnets. *J. Alloys Compd.* **2014**, *615*, S285−S290.

(18) Musiał, A.; Śniadecki, Z.; Idzikowski, B. Thermal stability and glass forming ability of amorphous $Hf_2Co_{11}B$ alloy. *Mater. Des.* **2017**, *114*, 404−409.

(19) McGuire, M. A.; Rios, O.; Ghimire, N. J.; Koehler, M. Hard ferromagnetism in melt-spun $Hf_2Co_{11}B$ alloys. *Appl. Phys. Lett.* **2012**, *101* (20), 202401.

(20) Balasubramanian, B.; Das, B.; Skomski, R.; Zhang, W. Y.; Sellmyer, D. J. Novel Nanostructured Rare-Earth-Free Magnetic Materials with High Energy Products. *Adv. Mater.* **2013**, *25* (42), 6090−6093.

(21) Balamurugan, B.; Das, B.; Zhang, W. Y.; Skomski, R.; Sellmyer, D. J. Hf−Co and Zr−Co alloys for rare-earth-free permanent magnets. *J. Phys.: Condens. Matter* **2014**, *26* (6), 064204.

(22) Yildiz, F.; Przybylski, M.; Ma, X. D.; Kirschner, J. Strong perpendicular anisotropy in $Fe_{1-x}Co_x$ alloy films epitaxially grown on mismatching Pd (001), Ir (001), and Rh (001) substrates. *Phys. Rev. B: Condens. Matter Mater. Phys.* **2009**, *80* (6), 064415.

(23) Burkert, T.; Nordström, L.; Eriksson, O.; Heinonen, O. Giant magnetic anisotropy in tetragonal FeCo alloys. *Phys. Rev. Lett.* **2004**, *93*, 027203.

(24) Kojima, T.; Ogiwara, M.; Mizuguchi, M.; Kotsugi, M.; Koganezawa, T.; Ohtsuki, T.; Tashiro, T. Y.; Takanashi, K. Fe−Ni composition dependence of magnetic anisotropy in artificially fabricated $L1_0$-ordered FeNi films. *J. Phys.: Condens. Matter* **2014**, *26*, 064207.

(25) Jiang, Y.; Liu, J.; Suri, P. K.; Kennedy, G.; Thadhani, N. N.; Flannigan, D. J.; Wang, J. P. Preparation of an α''-$Fe_{16}N_2$ Magnet via a Ball Milling and Shock Compaction Approach. *Adv. Eng. Mater.* **2016**, *18* (6), 1009−1016.

(26) Hermus, M.; Yang, M.; Grüner, D.; DiSalvo, F. J.; Fokwa, B. P. T. Drastic Change of Magnetic Interactions and Hysteresis through Site-Preferential Ru/Ir Substitution in $Sc_2FeRu_{5-x}Ir_xB_2$. *Chem. Mater.* **2014**, *26*, 1967−1974.

(27) Zhang, Y.; Miller, G. J.; Fokwa, B. P. T. Computation-al Design of Rare-Earth-Free Magnets with the $Ti_3Co_5B_2$-Type Structure. *Chem. Mater.* **2017**, *29*, 2535−2541.

(28) Blöchl, P. E. Projector augmented-wave method. *Phys. Rev. B: Condens. Matter Mater. Phys.* **1994**, *50*, 17953−17979.

(29) Kresse, G.; Joubert, D. From ultrasoft pseudopoten-tials to the projector augmented-wave method. *Phys. Rev. B: Condens. Matter Mater. Phys.* **1999**, *59*, 1758−1775.

(30) Kresse, G.; Furthmuller, J. Efficient iterative schemes for ab initio total-energy calculations using a plane-wave basis set. *Phys. Rev. B: Condens. Matter Mater. Phys.* **1996**, *54*, 11169−11186.

(31) Hafner, J. Ab-initio simulations of materials using VASP: Density-functional theory and beyond. *J. Comput. Chem.* **2008**, *29*, 2044−2078.

(32) Perdew, J. P.; Burke, K.; Ernzerhof, M. Generalized gradient approximation made simple. *Phys. Rev. Lett.* **1996**, *77* (18), 3865−3868.

(33) Shankhari, P.; Scheifers, J. P.; Hermus, M.; Yubuta, K.; Fokwa, B. P. T. Unexpected Trend Deviation in Isoelectronic Transition Metal Borides $A_3T_5B_2$ (A = group 4, T = group 9): $Ti_3Co_5B_2$-vs. Perovskite-Type Studied by Experiments and DFT Calculations. *Z. Anorg. Allg. Chem.* **2017**, *643* (21), 1551−1556.

(34) Shankhari, P. Combined Theory and Experiment Toward Designing and Preparing Itinerant Magnetic Transition Metal-Rich Borides of $Ti_3Co_5B_2$-type. Ph.D. Dissertation, UC Riverside, 2019.

(35) Scheifers, J. P.; Zhang, Y.; Fokwa, B. P. T. Boron: Enabling Exciting Metal-Rich Structures and Magnetic Properties. *Acc. Chem. Res.* **2017**, *50*, 2317−2325.

(36) Shankhari, P.; Zhang, Y.; Stekovic, D.; Itkis, M. E.; Fokwa, B. P. T. Unexpected Competition between Antiferromagnetic and Ferromagnetic States in $Hf_2MnRu_5B_2$: Predicted and Realized. *Inorg. Chem.* **2017**, *56* (21), 12674−12677.

(37) Shankhari, P.; Bakshi, N. G.; Zhang, Y.; Stekovic, D.; Itkis, M. E.; Fokwa, B. P. T. A delicate balance between antiferromagnetism and ferromagnetism: theoretical and experimental studies of $A_2MRu_5B_2$ (A = Zr, Hf; M = Fe, Mn) metal borides. *Chem. - Eur. J.* **2020**, *26*, 1979−1988.

(38) Dronskowski, R.; Bloechl, P. E. Crystal orbital Hamilton populations (COHP): energy-resolved visualization of chemical bonding in solids based on density-functional calculations. *J. Phys. Chem.* **1993**, *97*, 8617−8624.

https://dx.doi.org/10.1021/jacs.0c10778
J. Am. Chem. Soc. 2021, 143, 4205−4212

(39) Tank, R. W. J. O.; Jepsen, O.; Burkhardt, A.; Andersen, O. K. *TB-LMTO-ASA Program*, version 4.7. Max-Plank Institute for Solid-State Research: Stuttgart, Germany, 1994.
(40) Dronskowski, R.; Korczak, K.; Lueken, H.; Jung, W. Chemically tuning between ferromagnetism and antiferromagnetism by combining theory and synthesis in iron manganese rhodium borides. *Angew. Chem., Int. Ed.* **2002**, *41*, 2528−2532.
(41) Young, D. S.; Sachais, B. S.; Jefferies, L. C. *The Rietveld Method*; Oxford University Press: Oxford, 1993; pp 1−332.
(42) Rodriguez-Carvajal, J. *FullProf: A Program for Rietveld Refinement and Pattern Matching Analysis*; Abstract of the satellite meeting on powder diffraction of the XV congress of the IUCr, Toulouse, France, 1990, p 127.
(43) Brgoch, J.; Yeninas, S.; Prozorov, R.; Miller, G. J. Structure, bonding, and magnetic response in two complex borides: $Zr_2Fe_{1-\delta}Ru_{5+\delta}B_2$ and $Zr_2Fe_{1-\delta}(Ru_{1-x}Rh_x)_{5+\delta}B_2$. *J. Solid State Chem.* **2010**, *183*, 2917−2924.
(44) Hadimani, R. L.; Melikhov, Y.; Snyder, J. E.; Jiles, D. C. Determination of Curie temperature by Arrott plot technique in $Gd_5(Si_xGe_{1-x})_4$ for $x > 0.575$. *J. Magn. Magn. Mater.* **2008**, *320*, e696−e698.
(45) Zhu, H.; Ni, C.; Zhang, F.; Du, Y.; Xiao, J. Q. Fabrication and magnetic property of MnB alloy. *J. Appl. Phys.* **2005**, *97*, 10M512.
(46) Ma, S.; Bao, K.; Tao, Q.; Zhu, P.; Ma, T.; Liu, B.; Liu, Y.; Cui, T. Manganese mono-boride, an inexpensive room temperature ferromagnetic hard material. *Sci. Rep.* **2017**, *7*, 43759.

https://dx.doi.org/10.1021/jacs.0c10778
J. Am. Chem. Soc. 2021, 143, 4205−4212